Wrench-feasible workspace and stiffness characteristics of revolute and antiparallelogram tensegrity joints

Vimalesh Muralidharan

Wrench-feasible workspace and stiffness characteristics of revolute and antiparallelogram tensegrity joints

Vimalesh Muralidharan

Abstract

This technical report details the derivation of the static models of two antagonistically actuated joints: revolute (R) joint and antiparallelogram (X) joint. The wrench-feasible workspace (WFW) and stiffness characteristics of these joints are studied with numerical examples. Based on this study, several templates have been considered for the WFW for these joints. The nature of joint stiffness in each of these templates is characterized in a case-wise manner. Finally, a WFW template that is most suitable for designing these joints is identified.

1 Organization of the report

Two antagonistically actuated joints namely, the revolute joint or the R-joint and the antiparallelogram joint, also referred to as the X-joint, are studied in this report. The analysis of the R-joint is carried out in Section 2, and the X-joint in Section 3. The organization of each of these sections are identical and are detailed in the following. Firstly, a generalized coordinate is identified to describe the configuration of the joint, and all the dependent coordinates are obtained in terms of this coordinate for further study. This is followed by static analysis of the joint, where the expression of total potential energy is derived, followed by the equation of static equilibrium and stiffness. Based on the study of numerical examples, several workspace templates have been proposed and their respective stiffness behaviors are characterized in each case. Finally, the conclusion of this study is presented in Section 4.

2 R-joint

A schematic of the R-joint is shown in Fig. 1. It consists of two congruent isosceles triangles, one on top of another, connected by a revolute joint at point $\boldsymbol{o}$. The joint is equipped with two identical springs (spring constant, k) on either side to impart stiffness into the system. It is actuated by two cables passing through the middle of the springs, by applying forces, F_1 and F_2, respectively. Additionally, a point mass M is attached to the segment $\boldsymbol{p}_1\boldsymbol{p}_2$ at a distance d. The linear mass density (i.e., mass per unit length) of the links is given by ρ.

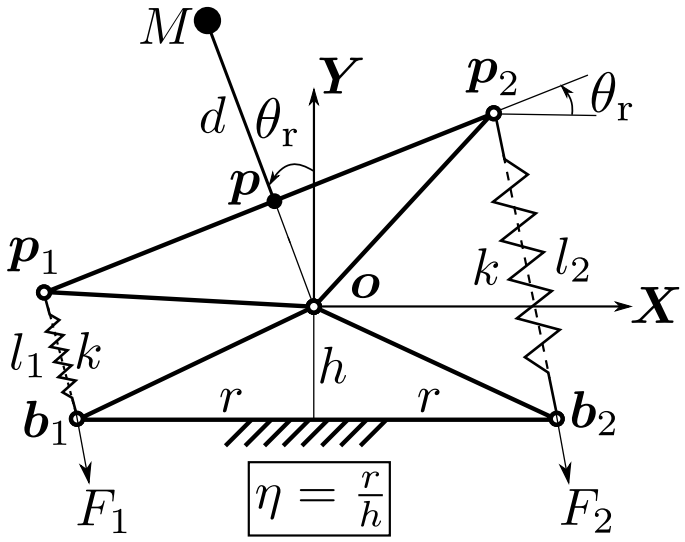

Figure 1: Schematic of the revolute joint.

The generalized coordinate that measures the orientation of the joint w.r.t. the vertical is given by θ_r. The dependent coordinates l_1 and l_2 are expressed as a function of θ_r, for further use in the upcoming sections. The following relations can be obtained using elementary geometric principles:

$$l_1 = 2\left(h\cos\frac{\theta_\mathrm{r}}{2} - r\sin\frac{\theta_\mathrm{r}}{2}\right), \quad l_2 = 2\left(h\cos\frac{\theta_\mathrm{r}}{2} + r\sin\frac{\theta_\mathrm{r}}{2}\right). \tag{1}$$

The derivatives of l_1, l_2 w.r.t. θ_r are:

$$\frac{\mathrm{d}l_1}{\mathrm{d}\theta_\mathrm{r}} = -\left(h\sin\frac{\theta_\mathrm{r}}{2} + r\cos\frac{\theta_\mathrm{r}}{2}\right), \quad \frac{\mathrm{d}l_2}{\mathrm{d}\theta_\mathrm{r}} = \left(-h\sin\frac{\theta_\mathrm{r}}{2} + r\cos\frac{\theta_\mathrm{r}}{2}\right); \tag{2}$$

$$\frac{\mathrm{d}^2l_1}{\mathrm{d}\theta_\mathrm{r}^2} = \frac{1}{2}\left(-h\cos\frac{\theta_\mathrm{r}}{2} + r\sin\frac{\theta_\mathrm{r}}{2}\right), \quad \frac{\mathrm{d}^2l_2}{\mathrm{d}\theta_\mathrm{r}^2} = -\frac{1}{2}\left(h\cos\frac{\theta_\mathrm{r}}{2} + r\sin\frac{\theta_\mathrm{r}}{2}\right). \tag{3}$$

2.1 Limits of motion of the R-joint due to singularities

The direction of the applied forces F_1 and F_2 are not defined when $l_1 = 0$ and $l_2 = 0$, respectively. Hence, it is not possible to control the manipulator in these configurations, and consequently, they define the boundaries of the wrench-feasible workspace (when no limits are imposed on the forces applied by the tendons) of the joint. This is illustrated in Fig. 2.

Cable-driven manipulators also suffer from force-closure singularities in addition to the singularities observed in parallel manipulators. Force-closure singularities refer to the configurations where the manipulator cannot withstand an arbitrary external wrench applied on one of the links, when all the cables are in tension and locked. For the R-joint, such situations occur when the line of action of force, l_1 or l_2 passes through the point $\boldsymbol{o}$ as illustrated in Fig. 3.

However, the limits of motion are defined by only one of these singularities, depending on the ratio $\frac{r}{h}$. From the Figs. 2 and 3, the following observations on the limits of motion can be made:

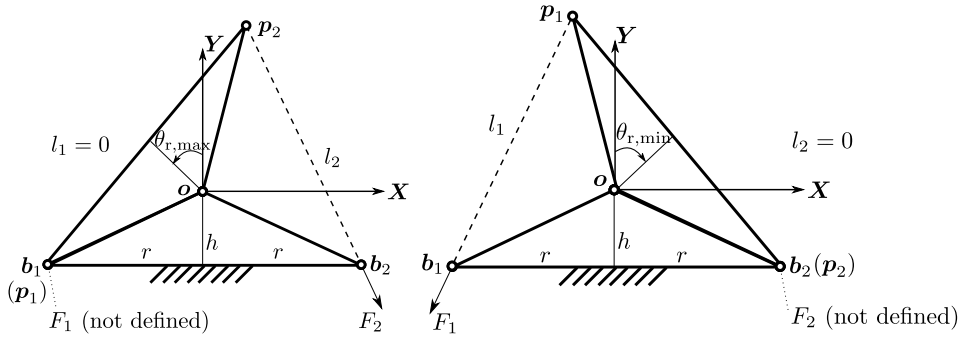

(a) Singularity for the first cable (b) Singularity for the second cable

Figure 2: Limits of motion for the R-joint due to the vanishing of l_1 and l_2.

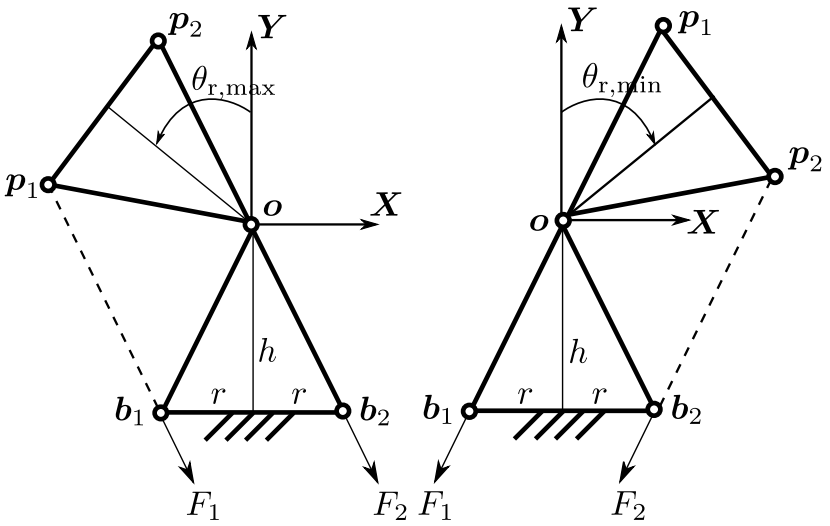

(a) Singularity for the second cable (b) Singularity for the first cable

Figure 3: Limits of motion for the R-joint due to force-closure singularity.

- Case 1 ($r > h$): The limit of motion is formed by $l_i = 0, i = 1, 2$, leading to: $\theta_{\mathrm{r}} \in (-\left(\pi - 2\tan^{-1}\left(\frac{r}{h}\right)\right), \left(\pi - 2\tan^{-1}\left(\frac{r}{h}\right)\right)$.
- Case 2 ($r < h$): Occurrence of force-closure singularity limits the motion, leading to: $\theta_{\mathrm{r}} \in \left(-2\tan^{-1}\left(\frac{r}{h}\right), 2\tan^{-1}\left(\frac{r}{h}\right)\right)$
- Case 3 ($r = h$): Limit of motion is formed by both $l_i = 0, i = 1, 2$ and force-closure singularity simultaneously: $\theta_{\mathrm{r}} \in \left(-\frac{\pi}{2}, \frac{\pi}{2}\right)$. The amplitude of singularity free motion is maximum in this case.

2.2 Static analysis of the R-joint

In this section, the equation of static equilibrium and stiffness of the R-joint are obtained using the potential energy approach. The expression of total potential energy of the joint is obtained as the sum of potential due to gravity (U_{g}), springs (U_{sp}), and external forces applied by the tendons (U_{f}), which are computed as follows:

- Gravitational potential: Setting the zero potential to be along the X axis, the potential due to gravity is obtained as follows:

$$U_{\mathrm{g}} = 2\rho g\left(r + \sqrt{r^2 + h^2}\right) y_c \cos\theta_{\mathrm{r}} + Mg(d + h)\cos\theta_{\mathrm{r}}, \tag{4}$$

  where $y_c = \frac{h\left(2r+\sqrt{r^2+h^2}\right)}{2\left(r+\sqrt{r^2+h^2}\right)}$ is the distance of the center of mass (COM) of the moving triangle from $\boldsymbol{o}$. Substituting the expression of y_c in Eq. (4), results in:

$$U_{\mathrm{g}} = \rho g\left(2r + \sqrt{r^2 + h^2}\right)\cos\theta_{\mathrm{r}} + Mg(d + h)\cos\theta_{\mathrm{r}}. \tag{5}$$

- Elastic potential due to springs: Assuming zero free-lengths for the springs, the spring potential may be computed as follows:

$$U_{\mathrm{sp}} = \frac{1}{2}k\left(l_1^2 + l_2^2\right) = 2k\left(r^2 + h^2 - \left(r^2 - h^2\right)\cos\theta_{\mathrm{r}}\right). \tag{6}$$

- Work potential due to tendons/cables: Potential due to actuation forces are computed as:

$$U_{\mathrm{f}} = F_1 l_1 + F_2 l_2 = 2F_1\left(h\cos\frac{\theta_{\mathrm{r}}}{2} - r\sin\frac{\theta_{\mathrm{r}}}{2}\right) + 2F_2\left(h\cos\frac{\theta_{\mathrm{r}}}{2} + r\sin\frac{\theta_{\mathrm{r}}}{2}\right). \tag{7}$$

Hence, the total potential energy of the R-joint is obtained to be:

$$U_{\mathrm{r}} = U_{\mathrm{g}} + U_{\mathrm{sp}} + U_{\mathrm{f}}, \tag{8}$$

$$\begin{aligned} U_{\mathrm{r}} =& \rho g h\left(2r + \sqrt{r^2 + h^2}\right)\cos\theta_{\mathrm{r}} + Mg(d + h)\cos\theta_{\mathrm{r}} + 2k\left(r^2 + h^2 - \left(r^2 - h^2\right)\cos\theta_{\mathrm{r}}\right) \\ &+ 2F_1\left(h\cos\frac{\theta_{\mathrm{r}}}{2} - r\sin\frac{\theta_{\mathrm{r}}}{2}\right) + 2F_2\left(h\cos\frac{\theta_{\mathrm{r}}}{2} + r\sin\frac{\theta_{\mathrm{r}}}{2}\right). \end{aligned} \tag{9}$$

Differentiation of the total potential (U_r) w.r.t. θ_r leads to the equation of static equilibrium, which is of the form: $G_\mathrm{r} = \Gamma_\mathrm{r}$, where:

$$G_\mathrm{r} = C \sin\theta_\mathrm{r}, \text{ with } C = \left(2k\left(r^2 - h^2\right) - g\left(M(d+h) + h\rho\left(\sqrt{h^2+r^2} + 2r\right)\right)\right), \tag{10}$$

$$\Gamma_\mathrm{r} = -F_1\frac{\mathrm{d}l_1}{\mathrm{d}\theta_\mathrm{r}} - F_2\frac{\mathrm{d}l_2}{\mathrm{d}\theta_\mathrm{r}} = F_1\left(h\sin\frac{\theta_\mathrm{r}}{2} + r\cos\frac{\theta_\mathrm{r}}{2}\right) + F_2\left(h\sin\frac{\theta_\mathrm{r}}{2} - r\cos\frac{\theta_\mathrm{r}}{2}\right). \tag{11}$$

The symbol G_r represents the wrench due to gravity and the springs, while Γ_r represents the external wrench that can be provided by the tendons. Using Eq. (2), it can be shown that the coefficients of F_1 and F_2 are positive and negative, respectively, within the limits of motion in all the cases listed in Section 2.1. This result is also intuitive from Fig. 1, as it is apparent that F_1 applies an anticlockwise moment, and F_2 a clockwise moment on the joint, respectively.

Also, the forces provided by the cables are limited physically, leading to: $F_1, F_2 \in [F_\mathrm{min}, F_\mathrm{max}]$. Since the coefficient of F_1 (resp. F_2) in Γ_r is always positive (resp. negative), the maximal (resp. minimal) boundary of the available wrench Γ_max (resp. Γ_min) is obtained when $F_1 = F_\mathrm{max}$ and $F_2 = F_\mathrm{min}$ (resp. $F_1 = F_\mathrm{min}$ and $F_2 = F_\mathrm{max}$). Considering these limits on Γ_r, it follows that the equation of static equilibrium can be satisfied only when: $G_\mathrm{r} \in [\Gamma_\mathrm{min}, \Gamma_\mathrm{max}]$. A numerical illustration of the plot of wrench boundaries ($\Gamma_\mathrm{min}, \Gamma_\mathrm{max}$), and the curve G_r are shown in Fig. 4(a).

The expression of stiffness of the joint is obtained by considering the second derivative of the total potential function w.r.t. θ_r as follows:

$$K_\mathrm{r} = \frac{\mathrm{d}G_\mathrm{r}}{\mathrm{d}\theta_\mathrm{r}} + F_1\frac{\mathrm{d}^2 l_1}{\mathrm{d}\theta_\mathrm{r}^2} + F_2\frac{\mathrm{d}^2 l_2}{\mathrm{d}\theta_\mathrm{r}^2}, \tag{12}$$

$$K_\mathrm{r} = C\cos\theta_\mathrm{r} + \frac{1}{2}F_1\left(-h\cos\frac{\theta_\mathrm{r}}{2} + r\sin\frac{\theta_\mathrm{r}}{2}\right) - \frac{1}{2}F_2\left(h\cos\frac{\theta_\mathrm{r}}{2} + r\sin\frac{\theta_\mathrm{r}}{2}\right). \tag{13}$$

It is essential to account for the static equilibrium equation ($G_\mathrm{r} = \Gamma_\mathrm{r}$) also while evaluating the stiffness of the joint at any orientation. Since the R-joint is redundantly actuated with two cables, it is capable of exhibiting a range of stiffness values at a given orientation. As a numerical example, the stiffness bounds for the joint parameters listed in Fig. 4(a), are shown in Fig. 4(b). The corresponding forces values are also indicated on the boundaries. It is observed that on the lower boundary of stiffness, at least one of the forces is equal to its allowed maximum of F_max, which shows that the actuation forces have a negative impact on the joint stiffness. A formal proof of this observation is not presented in this report for want of space.

From Eqs. (10), (11), and (13), it is observed that replacing θ_r by $(-\theta_\mathrm{r})$ and interchanging F_1 and F_2, results in the same respective expressions. This implies that only F_1 and F_2 interchange their roles, as the joint moves from the positive half of its workspace ($\theta_\mathrm{r} > 0$) to the negative half ($\theta_\mathrm{r} < 0$), while the distribution of stiffness remains unaffected. This is a consequence of the symmetry in the architecture as well as the actuation scheme of the joint (see Fig. 1). Thus, studying just one half of the problem, say, $\theta_\mathrm{r} \geq 0$ is sufficient to understand the behavior of the joint throughout its workspace. It will be shown that ($F_1 \geq F_2$) is necessary when $\left(\theta_\mathrm{r} \in \left]0, \frac{\pi}{2}\right[\right)$, if

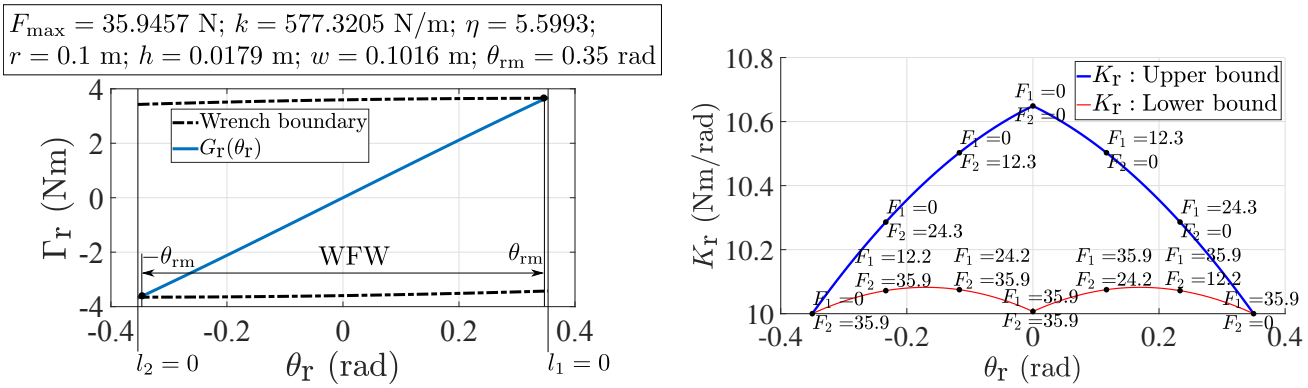

(a) Plot of G_r and wrench boundary

(b) Stiffness bounds

Figure 4: Wrench-feasible workspace (left) and stiffness bounds (right) for the R-joint.

the stiffness (K_r) is specified to be positive. Using this information, the templates for WFW will be studied, subsequently.

2.3 Proof for $(F_1 \geq F_2)$ when $K_r > 0$ and $\theta_r \geq 0$

Since K_r must be positive for all admissible combinations of forces inside the WFW, it follows that stiffness must also be positive when $\theta_r = 0, F_1 = 0, F_2 = 0$. Substituting these values into the expression in Eq. (13), leads to the condition: $C > 0$, which must be satisfied always. From the expression of C in Eq. (10), this requires $(r > h)$ to be satisfied.

The expressions in Eqs. (10), (11), and (13) can be rewritten in a simplified form as follows:

$$2Ccs - rF^- c - hF^+ s = 0, \tag{14}$$

$$K_r = C(c^2 - s^2) + \frac{1}{2} rF^- s + \frac{1}{2} hF^+ c > 0, \tag{15}$$

where $c = \cos\frac{\theta_r}{2}, s = \sin\frac{\theta_r}{2}, F^+ = F_1 + F_2$, and $F^- = F_1 - F_2$. Since it is known that the positive half of WFW must be limited by $\left(\theta_r < \frac{\pi}{2}\right)$ due to singularities, it is observed that $(c > s)$. Solving for F^+ from Eq. (14) and substituting into the expression in Eq. (15), leads to the condition:

$$F^- > \frac{2Cs^3}{r}. \tag{16}$$

Since it has been shown that $C > 0$ must be satisfied, it is clear from the above condition that $F^- > 0$, or $F_1 > F_2$.

2.4 Templates for the WFW boundary of R-joint

This section aims at finding a suitable workspace template that can be used in a design process when the stiffness is specified to be positive throughout the WFW. By studying several numerical examples, three general cases were observed in the plot of G_r and bounds of Γ_r. These are shown

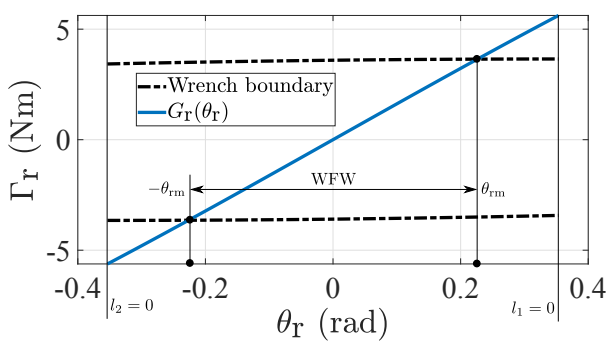

(a) Template 1

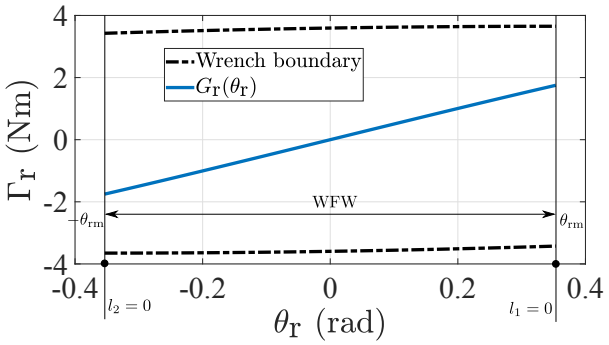

(b) Template 2

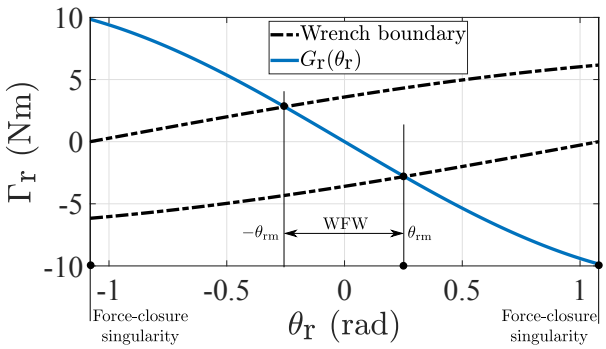

(c) Template 3

Figure 5: Templates of WFW for R-joint.

in Fig. 5. In templates 1 and 3, it is found that the WFW is bounded by the intersection of the curves G_{r} and bounds of Γ_{r}. While, in template 2 the WFW is bounded by singularities ($l_1, l_2 = 0$). In the latter situation, it is possible to reduce the limit of actuation forces ($F_{\max}$) till an intersection happens between the curve G_{r} and the wrench boundary. Such a change would not affect the size of WFW, but would increase the stiffness of the joint which is desirable. Thus, when a minimum $F_{\max}$ is required in the design process, WFW template 2 is not favorable.

From Fig. 5(c), it is found that the slope of G_{r} w.r.t. θ_{r} is negative at rest (i.e., when $F_1 = F_2 = 0, \Gamma_{\mathrm{r}} = 0$). From Eq. (12), this implies that the stiffness is negative at rest and hence this template is also unsuitable for the design process.

The issues pointed out with templates 2 and 3 are not present in template 1, where the positive boundary of WFW is formed by the intersection of G_{r} with $\Gamma_{\max}$. Hence, it is regarded as the most favorable choice in a design process aimed at minimizing the actuation forces, while ensuring that the joint is able to reach the prescribed WFW with a minimum specified (positive) stiffness throughout.

3 X-joint

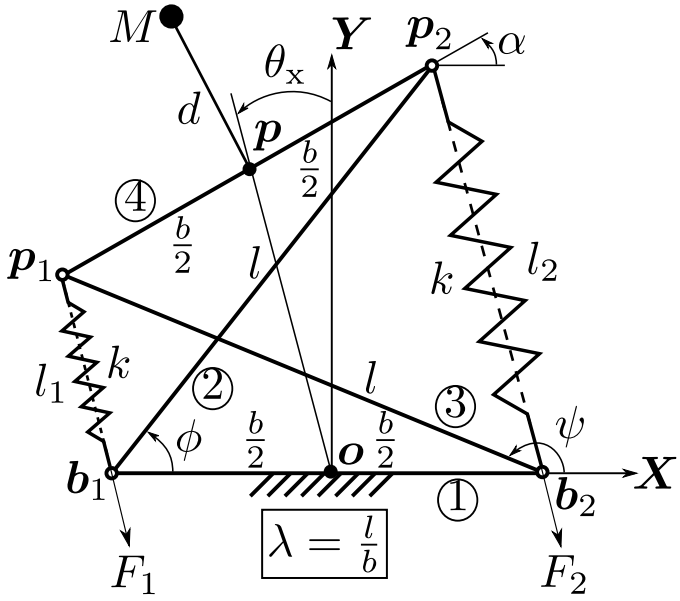

Figure 6: Schematic of the X-joint.

The schematic of the X-joint is shown in Fig. 6. It contains three moving links $2, 3, 4$ and one fixed link 1. The top and bottom bars $(1, 4)$ are of length b, while the crossed bars $(2, 3)$ are of length l. It is noted that the condition, $l > b$ must be satisfied for the assembly of the joint. The other parameters k, ρ, M, d, F_1, F_2 possess the same definitions as in the case of the R-joint (see Section 2).

The configuration of the X-joint is denoted by the orientation angle (θ_{X}) of the segment connecting the midpoints of the bars 1 and 4 w.r.t. the vertical (see Fig. 6). All the other dependent coordinates can be expressed as a function of θ_{X}, using elementary geometric principles, as follows:

$$\begin{aligned}
&\alpha = 2\theta_{\mathrm{X}};\\
&\cos\phi = \frac{\left(b\cos^2\theta_{\mathrm{X}} - \sin\theta_{\mathrm{X}}\sqrt{l^2 - b^2\cos^2\theta_{\mathrm{X}}}\right)}{l}; \quad \sin\phi = \frac{\left(b\sin\theta_{\mathrm{X}} + \sqrt{l^2 - b^2\cos^2\theta_{\mathrm{X}}}\right)}{l};\\
&\cos\psi = -\frac{\left(b\cos^2\theta_{\mathrm{X}} + \sin\theta_{\mathrm{X}}\sqrt{l^2 - b^2\cos^2\theta_{\mathrm{X}}}\right)}{l}; \quad \sin\psi = \frac{\left(-b\sin\theta_{\mathrm{X}} + \sqrt{l^2 - b^2\cos^2\theta_{\mathrm{X}}}\right)}{l};\\
&l_1 = -b\sin\theta_{\mathrm{X}} + \sqrt{l^2 - b^2\cos^2\theta_{\mathrm{X}}}; \quad l_2 = b\sin\theta_{\mathrm{X}} + \sqrt{l^2 - b^2\cos^2\theta_{\mathrm{X}}}.
\end{aligned} \tag{17}$$

Differentiation of l_1 and l_2 w.r.t. θ_{X} yields:

$$\frac{\mathrm{d}l_1}{\mathrm{d}\theta_{\mathrm{X}}} = b\cos\theta_{\mathrm{X}}\left(\frac{b\sin\theta_{\mathrm{X}}}{\sqrt{l^2 - b^2\cos^2\theta_{\mathrm{X}}}} - 1\right); \quad \frac{\mathrm{d}l_2}{\mathrm{d}\theta_{\mathrm{X}}} = b\cos\theta_{\mathrm{X}}\left(\frac{b\sin\theta_{\mathrm{X}}}{\sqrt{l^2 - b^2\cos^2\theta_{\mathrm{X}}}} + 1\right). \tag{18}$$

Further differentiation w.r.t. θ_{X} results in:

$$\frac{\mathrm{d}^2l_1}{\mathrm{d}\theta_{\mathrm{X}}^2} = b\left(\frac{bl^2\cos 2\theta_{\mathrm{X}} - b^3\cos^4\theta_{\mathrm{X}}}{\left(l^2 - b^2\cos^2\theta_{\mathrm{X}}\right)^{3/2}} + \sin\theta_{\mathrm{X}}\right); \quad \frac{\mathrm{d}^2l_2}{\mathrm{d}\theta_{\mathrm{X}}^2} = b\left(\frac{bl^2\cos 2\theta_{\mathrm{X}} - b^3\cos^4\theta_{\mathrm{X}}}{\left(\lambda^2 - b^2\cos^2\theta_{\mathrm{X}}\right)^{3/2}} - \sin\theta_{\mathrm{X}}\right). \tag{19}$$

Unlike the R-joint, the motion of the X-joint is always limited by the occurrence of parallel singularities at $\theta_{\mathrm{X}} = \pm\frac{\pi}{2}$, irrespective of the dimensions of the links.

3.1 Static analysis of the X-joint

The expression for total potential energy of the X-joint is obtained in a manner similar to that of the R-joint, as:

$$U_{\mathrm{x}} = -\cos 2\theta_{\mathrm{X}}\left(b^2k - dgM\right) + (\rho(b+l)+M)g\cos\theta_{\mathrm{X}}\sqrt{l^2 - b^2\cos^2\theta_{\mathrm{X}}} + kl^2 + F_1l_1 + F_2l_2. \tag{20}$$

Differentiating the total potential energy w.r.t. θ_{X} leads to the equation of static equilibrium: $G_{\mathrm{x}} = \Gamma_{\mathrm{x}}$, with:

$$G_{\mathrm{x}} = C_1\sin 2\theta_{\mathrm{X}} + \frac{C_2\sin\theta_{\mathrm{X}}\left(2b^2\cos^2\theta_{\mathrm{X}} - l^2\right)}{b\sqrt{l^2 - b^2\cos^2\theta_{\mathrm{X}}}}, \text{ where } C_1 = 2(b^2k - Mgd), C_2 = bg(M + \rho(b+l)), \tag{21}$$

$$\Gamma_{\mathrm{x}} = -F_1\frac{\mathrm{d}l_1}{\mathrm{d}\theta_{\mathrm{X}}} - F_2\frac{\mathrm{d}l_2}{\mathrm{d}\theta_{\mathrm{X}}} = F_1b\cos\theta_{\mathrm{X}}\left(\frac{\sqrt{l^2 - b^2\cos^2\theta_{\mathrm{X}}} - b\sin\theta_{\mathrm{X}}}{\sqrt{l^2 - b^2\cos^2\theta_{\mathrm{X}}}}\right) - F_2b\cos\theta_{\mathrm{X}}\left(\frac{\sqrt{l^2 - b^2\cos^2\theta_{\mathrm{X}}} + b\sin\theta_{\mathrm{X}}}{\sqrt{l^2 - b^2\cos^2\theta_{\mathrm{X}}}}\right). \tag{22}$$

The symbols G_{x} and Γ_{x} possess the same physical meaning as in case of the R-joint. It can be shown that the coefficient of F_1 in the expression of Γ_{x}, is positive from the assembly condition $l > b$ and the following argument: $b\sqrt{\frac{l^2}{b^2} - \cos^2\theta_{\mathrm{X}}} > b\sin\theta_{\mathrm{X}} (= b\sqrt{1 - \cos^2\theta_{\mathrm{X}}})$. Also, from Eq. (22), it is

clear that the coefficient of F_2 is negative. This shows that the upper bound of Γ_{x} is obtained when $F_1 = F_{\max}, F_2 = F_{\min}$ and the lower bound when $F_1 = F_{\min}, F_2 = F_{\max}$.

The expression of stiffness of the joint is obtained by computing the second derivative of the total potential function w.r.t. θ_{X} as follows:

$$\begin{aligned} K_{\mathrm{x}} =& \frac{\mathrm{d}(G-\Gamma)}{\mathrm{d}\theta_{\mathrm{X}}} = \frac{\mathrm{d}G}{\mathrm{d}\theta_{\mathrm{X}}} + F_1 \frac{\mathrm{d}^2 l_1}{\mathrm{d}\theta_{\mathrm{X}}^2} + F_2 \frac{\mathrm{d}^2 l_2}{\mathrm{d}\theta_{\mathrm{X}}^2} \\ =& 2C_1 \cos 2\theta_{\mathrm{X}} - \frac{C_2 \cos\theta_{\mathrm{X}} \left(\left(l^2 - b^2 \cos 2\theta_{\mathrm{X}}\right)^2 - b^2 \left(l^2 - b^2\right) \cos 2\theta_{\mathrm{X}} \right)}{b \left(l^2 - b^2 \cos^2\theta_{\mathrm{X}}\right)^{3/2}} \\ &+ bF_1 \left(\frac{bl^2 \cos 2\theta_{\mathrm{X}} - b^3 \cos^4\theta_{\mathrm{X}}}{\left(l^2 - b^2 \cos^2\theta_{\mathrm{X}}\right)^{3/2}} + \sin\theta_{\mathrm{X}} \right) + bF_2 \left(\frac{bl^2 \cos 2\theta_{\mathrm{X}} - b^3 \cos^4\theta_{\mathrm{X}}}{\left(\lambda^2 - b^2 \cos^2\theta_{\mathrm{X}}\right)^{3/2}} - \sin\theta_{\mathrm{X}} \right). \end{aligned} \tag{23}$$

Similar to that of R-joint, the X-joint also exhibits symmetry about $\theta_{\mathrm{x}} = 0$, in which F_1 and F_2 interchange their respective roles in the positive and negative halves of the WFW. Therefore, for the X-joint also studying just the positive half of the WFW, $\theta_{\mathrm{x}} \geq 0$ is sufficient. Additionally it is recalled that $(l > b)$ or $(\lambda(= \frac{l}{b}) > 1)$ is necessary for the assembly of the joint.

As in the case of R-joint, the WFW and the stiffness bounds for the X-joint are illustrated with an examples in Fig. 7. From Fig, 7(a), it is observed that the WFW is formed by three disconnected regions, $\theta_{\mathrm{xm}} \in [-\theta_{\mathrm{xm}}, \theta_{\mathrm{xm}}]$ and two smaller isolated regions near the flat singularities $(\theta_{\mathrm{x}} = \pm\frac{\pi}{2})$. A "jump" from one region to another could be possible with a suitable dynamic trajectory might be possible, but those isolated regions are very small and are associated with unstable equilibrium configurations or negative stiffness. Thus, only the central portion would be considered as the WFW of this manipulator, in further study. The stiffness bounds are plotted for $\theta_{\mathrm{x}} \in [-\theta_{\mathrm{xm}}, \theta_{\mathrm{xm}}]$ in Fig. 7(b). Contrary to the observation made for R-joint, the effect of forces on stiffness turns out to be positive for the X-joint.

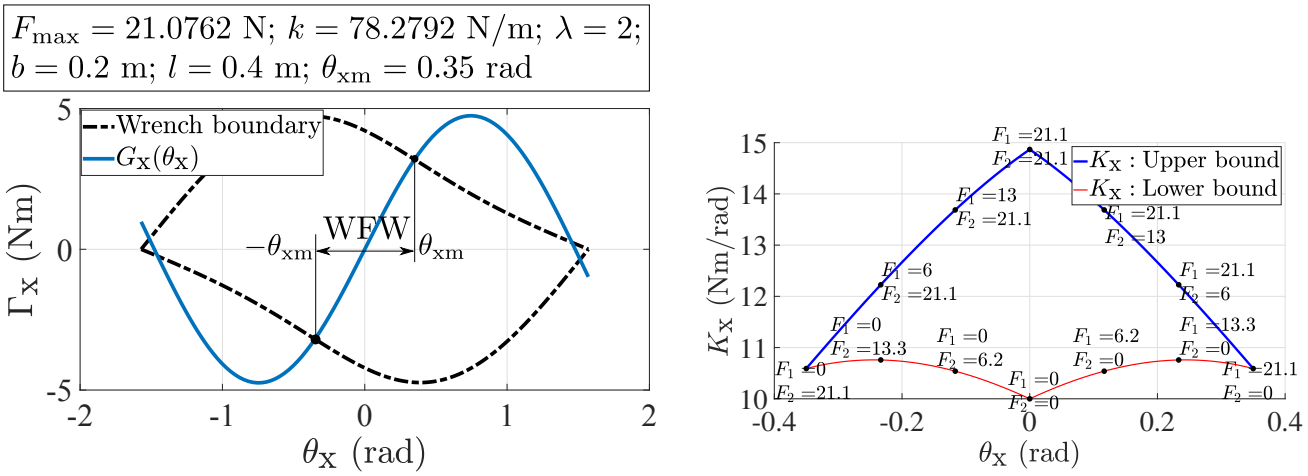

(a) Plot of G_{x} and wrench boundary

(b) Stiffness bounds

Figure 7: Wrench-feasible workspace (left) and stiffness bounds (right) for the X-joint.

3.2 Proof for $(F_1 \geq F_2)$ when $K_{\mathbf{x}} > 0$ and $\theta_{\mathbf{x}} \geq 0$

The equilibrium equation and the stiffness expression can be rewritten as follows:

$$\frac{bcsF^+}{\sqrt{\lambda^2 - c^2}} - bcF^- + \frac{C_2 s\left(2c^2 - \lambda^2\right)}{\sqrt{\lambda^2 - c^2}} + 2csC_1 = 0, \tag{24}$$

$$K_{\mathrm{x}} = -\frac{bF^+\left(c^4 - c^2\lambda^2 + \lambda^2 s^2\right)}{\left(\lambda^2 - c^2\right)^{3/2}} + bsF^- + 2C_1\left(c^2 - s^2\right) - \frac{C_2 c\left(\left(-c^2 + \lambda^2 + s^2\right)^2 - \left(\lambda^2 - 1\right)\left(c^2 - s^2\right)\right)}{\left(\lambda^2 - c^2\right)^{3/2}} > 0. \tag{25}$$

where $F^+ = (F_1 + F_2)$, $F^- = (F_1 - F_2)$. In the context of X-joint, the substitutions: $c = \cos\theta_{\mathrm{x}}$, $s = \sin\theta_{\mathrm{x}}$ and $\lambda = \frac{l}{b}$, have been carried out to simplify the expressions. Solving for C_1 from Eq. (24) and substituting into the expression of stiffness in Eq. (25), results[1] in:

$$\frac{bc^2}{s}F^- - \frac{bc^2 s^2}{\left(\lambda^2 - c^2\right)^{3/2}}F^+ - \frac{\lambda^4 s^2}{c\left(\lambda^2 - c^2\right)^{3/2}}C_2 > 0. \tag{26}$$

Since it is known that $C_2 > 0$ (by definition in Eq. (21)) and $F^+ > 0$, it is observed that the second and third terms in Eq. (26) are both negative. On the other hand, the coefficient of F^- is found to be positive. Thus, in order to ensure that the left hand side (LHS) of Eq. (26) remains positive, F^- must necessarily be positive. In other words, when the stiffness is specified to be positive, it is necessary that $F_1 > F_2$ for the X-joint when $\theta_{\mathrm{x}} > 0$.

3.3 Templates for the WFW boundary of X-joint

This section aims at finding a suitable workspace template for the X-joint to be used in its design process. As in the case of R-joint, the stiffness is considered to be positive throughout the WFW. By studying several numerical examples, three general templates are found for the plot of G_{x} and bounds of Γ_{x}. These are shown in Fig. 8. In templates 2 and 3, the positive boundary of WFW is formed by the intersection of G_{x} with $\Gamma_{\min}$, where $F_2 > F_1$. But, from Section 3.2, it is known that $F_1 > F_2$ is necessary to ensure a positive stiffness in the right half of the WFW. Thus, it is clear that the stiffness would be negative at some parts of the WFW in templates 2 and 3, which makes them unfavorable for the design process. On the other hand, the central portion of WFW in template 1 is free from the issue of negative stiffness and is hence deemed suitable for the design process. In summary, for the X-joint the positive boundary of WFW must be formed by the intersection of G_{x} with $\Gamma_{\max}$ for the stiffness to be positive throughout the WFW.

[1] Alternatively, it is possible to eliminate F^+ using Eq. (24), as in the case of R-joint. But, one must account for the condition: $F^+ \geq 0$ along with the inequality from stiffness. This turned out to be difficult to handle, algebraically. On the other hand, since there are no constraints on the sign of C_1 (see Eq. (21)), its elimination does not add any conditions other than the one from stiffness.

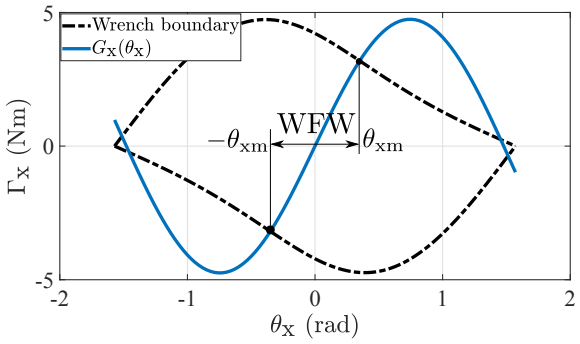

(a) Template 1

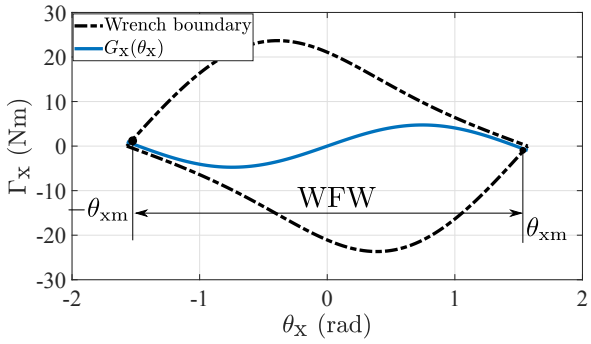

(b) Template 2

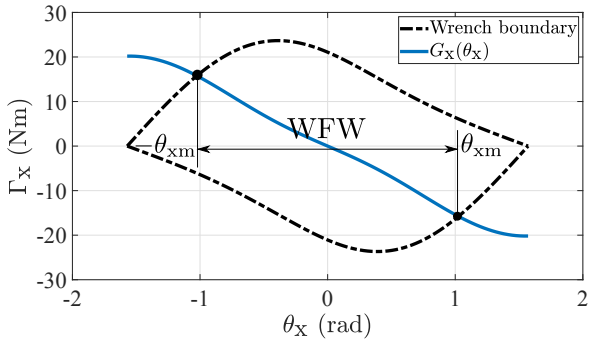

(c) Template 3

Figure 8: Templates of WFW for X-joint.

4 Conclusion

The static analysis of two antagonistically actuated joints with a point mass payload has been conducted in this study: the revolute (R) joint and the antiparallelogram (X) joint. For the R-joint, it is observed that the effect of applied forces on stiffness is negative. On the contrary, for the X-joint the effect of applied forces on stiffness is positive. For both the joints, it is found that the positive boundary of the wrench-feasible workspace (WFW) must be formed by the intersection of wrench due to internal potential (spring and gravity) and the upper bound of applied wrench, for the stiffness to be positive throughout the WFW and the actuation forces to be as low as possible.

Acknowledgement

This work was conducted with the support of the French National Research Agency (AVINECK Project ANR-16-CE33-0025).